

1 **Summer predictions of Arctic sea ice edge in multi-model seasonal re-forecasts**

2 Authors: Lauriane Batté⁽¹⁾, Ilona Välisuo⁽¹⁾, Matthieu Chevallier^(1,2), Juan C. Acosta Navarro⁽³⁾, Pablo
3 Ortega⁽³⁾ and Doug Smith⁽⁴⁾

4 **Abstract**

5 In this study, the forecast quality of 1993-2014 summer seasonal predictions of five global coupled
6 models, of which three are operational seasonal forecasting systems contributing to the Copernicus
7 Climate Change Service (C3S), is assessed for Arctic sea ice. Beyond the Pan-Arctic sea ice
8 concentration and extent deterministic re-forecast assessments, we use sea ice edge error metrics such
9 as the Integrated Ice Edge Error (IIEE) and Spatial Probability Score (SPS) to evaluate the advantages
10 of a multi-model approach.

11 Skill in forecasting the September sea ice minimum from late April to early May start dates is very
12 limited, and only one model shows significant correlation skill over the period when removing the
13 linear trend in total sea ice extent. After bias and trend-adjusting the sea ice concentration data, we
14 find quite similar results between the different systems in terms of ice edge forecast errors. The
15 highest values of September ice edge error in the 1993-2014 period are found for the sea ice minima
16 years (2007 and 2012), mainly due to a clear overestimation of the total extent. Further analyses of
17 deterministic and probabilistic skill over the Barents-Kara, Laptev-East Siberian and Beaufort-
18 Chukchi regions provide insight on differences in model performance.

19 For all skill metrics considered, the multi-model ensemble, whether grouping all five systems or only
20 the three operational C3S systems, performs among the best models for each forecast time, therefore
21 confirming the interest of multi-system initiatives building on model diversity for providing the best
22 forecasts.

23

24 **Affiliations:** (1) CNRM UMR 3589, Université de Toulouse, Météo-France, CNRS, Toulouse,
25 France; (2) Direction des Opérations pour la Prévision, Département Marine et Océanographie,
26 Météo-France, Toulouse, France; (3) Barcelona Supercomputing Centre (BSC), Barcelona, Spain; (4)
27 Met Office Hadley Centre, Exeter, UK

28

29 **Correspondence:** lauriane.batte@meteo.fr

30

31 ORCID (L Batté): 0000-0002-7903-9762

32 ORCID (I Välisuo): 0000-0002-8665-4990

33 ORCID (M. Chevallier): 0000-0003-2033-166X

34 ORCID (J. C. Acosta Navarro): 0000-0001-5375-0639

35 ORCID (P. Ortega): 0000-0002-4135-9621

36 ORCID (D. Smith): 0000-0001-5708-694X

37

38 **1. Introduction**

39

40 In recent decades, Arctic sea ice extent has significantly decreased, while exhibiting important year-
41 to-year variability, sparking interest in the polar prediction community in the provision of forecasts
42 for sea ice conditions at the sub-seasonal to decadal time scales.

43

44 Arctic sea ice extent anomalies have both local and remote impacts. At a local or regional scale, sea
45 ice formation or melt can have consequences on the livelihood of local communities, shipping
46 activities, fisheries and infrastructure safety (Eicken, 2013). Moreover, several works (see e.g. Vihma,
47 2014 and Jung et al. 2015 and references therein) have suggested evidence for remote effects of sea
48 ice cover on atmospheric variability in the midlatitudes, and the accelerated warming of the Arctic is
49 thought by some studies to bring more persistent Northern Hemisphere weather regimes favouring
50 extremes (Coumou et al. 2018, Francis et al. 2018), although this is still widely debated (Blackport et
51 al. 2019). One example of such remote effects is the link between autumn sea ice concentration over
52 the Barents-Kara seas and the subsequent winter North Atlantic Oscillation index which could explain
53 a significant part of climate variability over the North Atlantic sector at weekly to annual time scales
54 (Garcia-Serrano et al. 2015).

55

56 Mechanisms for Arctic sea ice predictability have been highlighted by past studies (see Guemas et al.
57 2016 for a review). These include the advection of anomalous sea ice conditions, the atmospheric
58 circulation over the Arctic, ocean heat transport and thermohaline circulation, but also persistence of
59 anomalies in the initial sea ice state. In the last decade, potential predictability studies using global
60 coupled models (GCMs) in a perfect model framework, such as that of the APPOSITE project
61 (Tietsche et al. 2014) have provided estimates of theoretical seasonal-to-decadal sea ice prediction
62 skill limits in current-generation climate models. Using different metrics, Day et al. (2014) and
63 Chevallier and Salas y Mélia (2012) estimated e-folding times of 2-5 months for total sea ice area in
64 GCMs, depending on the initial date, and consistent with that of observations such as NSIDC
65 (Blanchard-Wrigglesworth et al. 2011). For sea ice volume, significant levels of potential
66 predictability were found up to three years ahead (Day et al. 2014, Cruz-Garcia et al. 2019). Yet the
67 skill of initialized seasonal hindcasts often fall short of these potential predictability estimates
68 (Guemas et al. 2016).

69

70 Reliable prediction of total Arctic sea ice extent is in itself a challenge, but a correct sea ice extent
71 value may mask some large compensating errors in the presence or absence of ice. Indeed, sea ice
72 predictability and prediction skill may vary depending on the region of interest (Germe et al. 2014,
73 Bushuk et al. 2017), with different processes at play. Cruz-Garcia et al. (2019) highlighted using EC-

74 Earth perfect-model simulations that predictability in the Atlantic sector peripheral seas was linked to
75 local sea surface temperature and ocean heat content anomalies. In the case of summer sea ice
76 predictions, initial sea ice thickness is found to be a precursor for sea ice extent over the East Siberia,
77 Laptev, Beaufort and Chukchi Seas (Bushuk et al. 2017; Bushuk et al. 2019). To circumvent the
78 possible overestimation of skill using total sea ice extent, more challenging metrics that assess ice
79 edge errors were suggested by Goessling et al. (2016) and Goessling and Jung (2018) to evaluate
80 model skill in forecasting the position of the sea ice.

81

82 With thinning ice and a warmer atmosphere over the region, the melt season is particularly
83 challenging to forecast at such extended time ranges, where drivers of variability are dominated by
84 chaotic processes (Serreze and Stroeve, 2015; Olonscheck et al. 2019). Past studies have found that
85 SIE potential predictability estimated from GCM simulations drops faster in predictions initialized
86 from May than from July (Day et al. 2014), although these conclusions seem to be model-dependent
87 for the pan-Arctic SIE (see e.g. Bushuk et al. 2019). Bonan et al. (2019) found evidence for this loss
88 in predictive capacity in GCMs in the Arctic marginal seas between June and May starts by analyzing
89 correlation between sea ice area and sea ice volume from previous months of CMIP5 preindustrial
90 control runs. This springtime “predictability barrier” is also consistent with evaluations of empirical
91 forecasts based on observational data (Walsh et al. 2019). Moreover, initialized predictions often
92 perform at substantially lower skill levels than those estimated in potential predictability studies
93 (Guemas et al. 2016; Bushuk et al. 2019).

94

95 One approach to try and bridge the gap between potential and actual forecast skill is to combine
96 single-model forecasts into a multi-model ensemble. Since 2008, the Sea Ice Outlook initiative
97 (Blanchard-Wrigglesworth et al. 2017) has collected several sources of forecasts (statistical,
98 dynamical and heuristic) for the September Arctic sea ice minimum extent at three to one month lead
99 times. A recent study by Wayand et al. (2019) has demonstrated the current capabilities - and
100 limitations - of such state of the art forecasting systems in predicting sea ice concentration and
101 thickness during the 2018 melt season and the better performance of the multi-model on sub-seasonal
102 time scales. At the seasonal scale, past studies have demonstrated the interest of combining individual
103 forecasting systems into a multi-model ensemble for atmospheric fields (e.g. Hagedorn et al. 2005) as
104 a way of improving the signal-to-noise ratio of ensemble forecasts. Merryfield et al. (2013) showed
105 that the combination of CanSIPS and CFSv2 seasonal forecast systems led in most cases to improved
106 sea ice concentration forecast skill over the Arctic. Dirkson et al. (2019a) recently provided new
107 evidence of the additional skill of multi-model combinations over single models for September sea ice
108 concentration using six different state-of-the-art seasonal forecasting systems. In the framework of the
109 H2020-APPLICATE project, which aims to broaden the understanding of linkages between the Arctic
110 region and the Northern Hemisphere mid-latitudes and improve models over these regions, several

111 seasonal re-forecasts were run using state-of-the-art coupled climate models initialized in May and
112 November, over a period covering at least 22 years. These were evaluated alongside re-forecasts from
113 operational climate prediction centers involved in the project, contributing to the Copernicus Climate
114 Change Services (C3S) initiative. We focus here on predictions initialized at the end of April or May
115 to assess the skill of these models in forecasting summer Arctic sea ice concentration and extent
116 anomalies. We also further investigate the added value of a multi-model approach for sea ice forecasts
117 grouping the models from the APPLICATE project.

118

119 A complete description of the models and the skill metrics used for the evaluation is presented in
120 section 2. Section 3 describes the main results at a pan-Arctic scale, whereas section 4 focuses on
121 specific Arctic seas or regions. Limitations to the study and future developments for the different
122 forecast systems are discussed in section 5.

123

124 **2. Models and methods**

125

126 **2.1 Seasonal re-forecasts and reference data**

127

128 The present study focuses on boreal summer re-forecasts initialized on May 1 or late April. Seasonal
129 re-forecasts from five GCMs are evaluated: the model developed jointly by Centre National de
130 Recherches Météorologiques (CNRM) and Cerfacs for the sixth phase of the Coupled Model
131 Intercomparison Project (CMIP6) called CNRM-CM6-1; European Consortium Earth system model
132 version 3.2 (hereafter EC-Earth3.2), as well as re-forecasts provided in the framework of the
133 Copernicus Climate Change Service (C3S) from three operational systems: Met Office fifth global
134 seasonal forecasting system GloSea5, Météo-France sixth generation seasonal forecast system System
135 6 and the European Centre for Medium-Range Weather Forecasts fifth generation seasonal forecast
136 system SEAS5. Table 1 presents information on these different sets of seasonal re-forecasts regarding
137 the coupled model components, their resolution, and the initial conditions for the ocean and ice
138 components. All re-forecasts use the Nucleus for European Modelling of the Ocean (NEMO, Madec
139 et al. 2017) ocean model, albeit with different model versions and settings; however, the sea ice
140 components differ amongst the GCMs.

141

142 The CNRM-CM6-1 GCM is described in detail in Voltaire et al. (2019). This version of the GCM
143 uses Arpege-Climate v6.3 for the atmosphere and NEMO 3.6 – Gelato v6 for the ocean and sea ice.
144 The land surface component is Surfexv8. Coupling between atmosphere/land and ocean is called in
145 the Surfex interface using the OASIS-MCT code. This GCM was used to run seasonal re-forecast
146 experiments initialized on May 1st 1993-2014. An ensemble of 30 members was constructed by

147 combining three ocean and sea ice initial conditions with 10 initial perturbations of the ERA-Interim
148 atmospheric initial conditions for Arpege. The ocean and sea ice components are initialized from a
149 run constrained towards the Mercator Ocean International Glorys 2V4 reanalysis (Ferry et al. 2010),
150 using the same NEMO-Gelato model versions as in the GCM. The sea ice component adjusts to the
151 atmospheric forcing and ocean constraints, except for sea ice concentration which is relaxed towards
152 Glorys.

153

154 Re-forecasts from a second GCM, EC-Earth3.2, are also evaluated in this study. EC-Earth3.2 is based
155 on ECMWF's atmospheric circulation model IFS (cycle 36r4) and land surface model H-Tessel
156 coupled with the OASIS-3 coupler to the ocean model NEMO 3.6 including the Louvain-la-Neuve
157 Sea Ice Model LIM3 (Vancoppenolle et al., 2009). As for CNRM-CM6-1, re-forecasts are initialized
158 on May 1st 1993-2014. The ensemble size is of 10 members, generated with random perturbations of
159 ERA-Interim initial conditions. The LIM3 model is initialized in these re-forecasts using a standalone
160 NEMO-LIM3 run forced with atmospheric fluxes calculated from the Drakkar Forcing Set (DFS,
161 Brodeau et al., 2010), and assimilating sea ice concentrations using an Ensemble Kalman Filter
162 approach (Massonnet et al., 2014). The ocean initial conditions are interpolated from the ocean
163 reanalysis system ORAS4 reanalysis (Balmaseda et al., 2013).

164

165 Alongside these re-forecasts, three operational seasonal forecast systems from the Copernicus Climate
166 Change Service (C3S) are analyzed for the same forecast times. ECMWF SEAS5 (Johnson et al.,
167 2019) is based on the IFS cy43r1 atmospheric model directly coupled to the NEMO 3.4 ocean and
168 LIM2 sea ice (Fichefet et al., 1997) components. The 25-member ensemble is generated using both
169 initial condition and stochastic perturbations of the atmosphere. Ocean and sea ice are initialized from
170 the ocean reanalysis system ORA-S5 part of the operational OCEAN5 analysis (Zuo et al., 2019).

171

172 Met Office GloSea5 (MacLachlan et al. 2015) re-forecasts were also analyzed, building a 28-member
173 ensemble re-forecast from the 7-member ensembles initialized on the 9th, 17th, 25th of April and 1st
174 of May. GloSea5 also uses NEMO 3.4 but the Los Alamos sea ice model CICE 4.1. Note that these
175 two forecast systems use a higher resolution ocean and sea ice ($1/4^\circ$) than the other models in this
176 study.

177

178 A third system from the C3S program was also included in the analysis, Météo-France seasonal
179 forecast system 6 (MF-Sys6). This system is based on a very similar model version of the CNRM-CM
180 coupled model as CNRM-CM6-1 described previously, but runs at a higher resolution in the
181 atmosphere. 25 ensemble members are generated using atmospheric stochastic perturbations (Batté
182 and Déqué, 2016) and a lagged initialization, with 12 members initialized on the 20th of April, 12 on
183 the 25th of April, and one control member on the 1st of May. Ocean and sea ice initial conditions are

184 derived similarly to CNRM-CM6-1 from a run constrained towards Glorys 2V4, except for sea ice
185 concentration which evolves freely in the NEMO-Gelato run to initialize MF-Sys6.

186

187 Beyond the coupled GCMs used, the re-forecasts compared in this study use different initialization
188 strategies and ensemble generation techniques. This can impact the ensemble spread and forecast
189 quality.

190

191 The study evaluates monthly mean sea ice extent (SIE) derived from sea ice concentration (SIC),
192 using the 15% SIC threshold to define presence or absence of sea ice. These fields are compared to
193 reference data provided by the National Snow and Ice Data Center (NSIDC) version 4, based on
194 brightness temperature (Cavalieri et al. 1996).

195

196 Throughout the re-forecast period, NSIDC SIC data is missing in some areas north of 85°N. This
197 could have some influence on skill evaluations especially when computing area-averaged scores, we
198 therefore chose to consider gridpoint SIC data from 45°N to 85°N, masking out regions from 85°N to
199 90°N in our computations over the Pan-Arctic region.

200

201 **2.2 Re-forecast bias adjustment**

202

203 Due to model imperfection and initial error growth, re-forecasts based on GCMs are prone to
204 systematic errors and drift when forecast time increases. This makes bias adjustment of re-forecasts a
205 necessary step before the evaluation of forecast quality using the metrics described in the following
206 section.

207

208 For Pan-Arctic SIE, we chose to bias-correct the ensemble mean SIE of each individual model against
209 NSIDC using a leave-one-out cross-validation bias correction. The metrics shown therefore evaluate
210 the skill of the model SIE anomalies versus NSIDC SIE anomalies, irrespective of the mean SIE bias.

211

212 In the case of metrics based on Arctic sea ice edge position, we compare in this study two
213 straightforward methods for bias-adjusting the grid-point SIC values. The first method consists in
214 bias-correcting (BC) the SIC values using (as for total SIE) leave-one-out cross-validation against
215 NSIDC SIC. This simple method has some caveats, since for bounded fields such as SIC values it can
216 yield values outside the theoretical range. We simply correct “out of bounds” values by setting
217 negative SIC values to 0 and SIC values higher than 100% to 100%.

218

219 The second method uses also a leave-one-out cross-validation, but to trend-adjust (TA) the data: we
220 adjust the SIC of each model (either ensemble mean or member) at a given grid-point as well as

221 NSIDC data for a linear trend. In this study we chose to remove the linear trend and then compute
222 anomalies with respect to the 1993-2014 mean. The obtained SIC values are then adjusted to the [0,1]
223 range before computation of the indices described in the following section. Note that more elaborate
224 trend-adjustment techniques for SIC have been introduced in past works such as Dirkson et al.
225 (2019b).

226

227 **2.3 Re-forecast evaluation metrics**

228

229 After evaluating (and removing) the mean model biases for SIC and SIE with respect to NSIDC, two
230 types of verification metrics are used in this study. In section 3.2, total Pan-Arctic SIE re-forecast skill
231 is evaluated according to forecast time using standard deterministic scores such as root mean square
232 error (RMSE) and correlation. Benchmark skill for SIE is assessed using the persistence of April SIE
233 anomalies.

234

235 We then focus on the skill of the models in representing the position of the sea ice edge, using the
236 Integrated Ice Edge Error (IIEE, Goessling et al. 2016) and its probabilistic counterpart, the Spatial
237 Probability Score (SPS, Goessling and Jung, 2018). These metrics take into account possible error
238 compensations between overestimation and underestimation of the presence of ice over different
239 basins of the Arctic, and therefore present a more complete analysis of the ability of GCMs to predict
240 sea ice concentration at a seasonal time scale.

241

242 The IIEE is computed to evaluate the total spatial extent of errors in the position of the sea ice edge.
243 The IIEE is the sum of areas where the presence of sea ice, defined with a 15% SIC threshold, is
244 overestimated (O) and underestimated (U) with respect to reference data. Following Goessling et al.
245 (2016), the IIEE is decomposed into two terms, namely misplacement error (ME) and absolute extent
246 error (AEE), as follows:

247

$$248 \quad IIEE = O + U = |O - U| + 2 \cdot \min(O, U) = AEE + ME$$

249

250 The absolute error corresponds to the total Pan-Arctic SIE error when this metric is computed over the
251 region, whereas the misplacement error shows the compensation between areas with overestimation
252 and areas with underestimation.

253

254 In the case of the IIEE, two benchmark re-forecasts are considered depending on the bias-adjustment
255 technique used. The benchmark re-forecast IIEE is computed for comparison with bias corrected re-
256 forecasts (trend-adjusted re-forecasts, respectively) using a leave-one-out climatology (linear trend-
257 adjusted climatology, respectively) of SIC NSIDC data.

258

259 A natural extension to the IIEE is used to examine the skill of probabilistic forecasts for presence of
260 sea ice at a grid point level. The SPS consists of a spatial integral of the Brier Score for the
261 probabilistic event of SIC exceeding the 15% threshold. With NSIDC data as a reference, and under
262 the assumption that reference data is “perfect” and therefore not accounting for observational
263 uncertainty, the SPS is formulated as follows:

264

$$265 \quad SPS = \iint \left(P_{SIC_t > 0.15}(x, y) - 1_{SIC_o > 0.15}(x, y) \right)^2 dx dy$$

266

267 In this study, probabilities are computed by counting the fraction of ensemble members exceeding the
268 15% concentration threshold (with or without trend-adjustment), and then bias-corrected using leave-
269 one-out cross-validation. For the benchmark probability re-forecasts, we consider probabilities based
270 on the 21 other years of the re-forecast period, either with or without trend-adjustment.

271

272 The Brier Score (Brier, 1950) and its decomposition into reliability, resolution and uncertainty
273 components (Murphy, 1972) are computed over regional seas for the probabilistic event of SIC
274 exceeding the 15% concentration threshold. The positively-oriented Brier Skill Score (BSS) is used to
275 determine model skill over using a simple climatology to forecast this probability. In this framework,
276 reliability diagrams plotting binned forecast probabilities against mean observed frequencies for the
277 event help estimate the conditional bias in probability space of the ensembles, and quantify how
278 trustworthy these systems are on average over the re-forecast period (Weisheimer and Palmer, 2014).

279

280 Note that these metrics can be sensitive to the ensemble size of each model re-forecast, and
281 differences in skill should therefore be interpreted with caution - in particular, for the EC-Earth 3.2
282 model, 10 members were available, significantly less than the 25-30 member ensemble sizes of the
283 other models in this study.

284

285 **2.4 Multi-model combination**

286

287 The advantages of using a multi-model approach in seasonal forecasting have been demonstrated in
288 many studies focusing on the predictability of atmospheric fields (e.g. Hagedorn et al., 2005). We
289 compute here a simple multi-model combination of the different model re-forecasts by first bias-
290 adjusting each model individually (either with the BC or TA methods), and then combining the
291 members of each of the five models into an unweighted multi-model ensemble. This ensemble is
292 called MME in what follows. Most models studied have a similar ensemble size, except for the EC-
293 Earth 3.2 model. With the unweighted ensemble approach used in this study, this model is thus under-

294 represented with respect to the others in the MME.

295

296 Since two of the operational systems considered in this study show higher correlation values and
297 lower root mean square errors than in the other model re-forecasts, we also examine the skill of a
298 multi-model restricted to the operational C3S systems, called C3S MME.

299

300 **3. Pan-Arctic scale results**

301

302 This section describes the ability and deficiencies of current state-of-the-art seasonal forecasting
303 systems in reproducing summer Arctic sea ice concentration variability from May initializations.

304

305 **3.1 Systematic errors in sea ice concentration and extent**

306

307 Before focusing on integrated indices of hindcast quality, often computed after bias-correcting the
308 individual ensemble forecasts, we first assess the model quality in terms of systematic errors in the
309 raw model outputs for sea ice concentration.

310

311 Figure 1 shows the mean bias over the re-forecast period of month 1 (May) and month 5 (September)
312 SIC with respect to NSIDC. Red areas show where SIC is too low in the models, whereas blue areas
313 highlight where model have excessive SIC. All models show a common low bias in Labrador Sea
314 SIC, already present in the reanalyses used to initialize the re-forecasts (Chevallier et al. 2017).
315 Elsewhere, from the first month of simulation, the systems exhibit different behaviors. CNRM-CM6-1
316 has too low SIC along the ice edge in the Greenland sea, a feature shared with the operational MF-
317 Sys6 which relies on a similar version of the CNRM-CM coupled model and initial conditions of the
318 ocean and sea ice. The three other systems show too high SIC in the Iceland and Nordic seas at month
319 1. At longer lead times, both sets of re-forecasts based on CNRM-CM exhibit a substantially different
320 bias than the other models, with too little SIC over most of the Arctic. This is likely due to the
321 initialization strategy for the model, for which even at the initial stage, sea ice thickness is often too
322 low. During the melt season, this results in an excessive reduction of SIC over most of the Arctic, and
323 a subsequent loss in predictability. EC-Earth 3.2, SEAS5 and GloSea5 show similar patterns of
324 systematic errors for September, particularly over the Beaufort-Chukchi and East Siberian sectors
325 where SIC is too high at the end of the melt season. The largest differences between these three
326 models are found north of the Greenland, Iceland and Norwegian (GIN) seas and Barents-Kara seas in
327 September, where GloSea5 slightly under-estimates and SEAS5 slightly over-estimates SIC, while
328 EC-Earth 3.2 has biases of opposite sign between the Barents and Kara sectors.

329

330 So as to evaluate the impact of these biases on total Pan-Arctic SIE re-forecasts, as well as the model
331 spread 5 months after initialization, we show in Fig. 2 box-and-whisker plots of Pan-Arctic September
332 SIE computed with raw model outputs (before bias-correction) for SIC. For each year of the common
333 re-forecast period, the boxes show the interquartile range and spread of ensemble members, compared
334 to SIE computed from NSIDC SIC data. Alongside this analysis, we also compute the linear trend in
335 mean September SIE for each model as well as for NSIDC. Values are shown in Table 2.

336

337 The models exhibit different characteristics: consistent with results from Fig. 1, CNRM-CM6-1 (Fig.
338 2(a)) and MF-Sys6 (Fig. 2(e)) show a clear underestimation of September SIE for most years of the
339 re-forecast, whereas the three other models show values in the observed range. However, SEAS5 SIE
340 values are comparable to NSIDC in the beginning of the re-forecast period but are then overestimated
341 with respect to NSIDC after 2006, due to a too weak negative trend in the re-forecast (about one third
342 of the linear trend estimated in NSIDC). The four other models also underestimate the amplitude of
343 the negative trend, but much less so, with values ranging from -83,000 to -96,000 squared kilometers
344 per year of loss in Pan-Arctic SIE. This underestimation of the negative trend in SIE was also found,
345 although over a different re-forecast period and using a different model, by Wang et al. (2013). In the
346 case of GloSea5 and EC-Earth 3.2, SIE computed from NSIDC data are inside the range of the
347 ensemble for almost all years of the re-forecast period. The spread of SEAS5 appears to be slightly
348 lower than the other two operational seasonal re-forecast systems, GloSea5 and MF-Sys6. This could
349 be due to the burst initialization strategy for SEAS5, whereas the other systems used a lagged
350 ensemble approach with different ocean (and therefore sea ice) initial conditions.

351

352 Two consequences arise from these analyses. First of all, for most systems, it appears necessary to
353 bias-correct the SIC values since large systematic errors are found (sometimes related to errors
354 present from month 1 onwards). Second of all, the strong negative trend in SIC and hence SIE values
355 means that in skill scores such as correlation, the trend may have an impact on results. In Table 2,
356 results both with and without detrending SIE values are shown for each model and persistence of
357 April SIE anomalies. Although some models have very large biases which translate into high RMSE
358 before bias removal, they all exhibit correlation values before linear detrending above 0.65, with most
359 systems reaching approximately 0.8. However, when removing the linear trend, it appears that most of
360 this apparent skill is in fact related to correctly capturing the sign -and part of the amplitude -of the
361 trend over the region. Levels of skill unrelated to trend are much more modest.

362

363 Unless mentioned otherwise, the skill evaluations presented in what follows are therefore computed
364 for sea ice concentration ensemble re-forecasts that are linearly-detrended and bias corrected in cross-
365 validation mode, as described in section 2.2. At this stage, we note that the choice of a linear trend
366 may have some influence on results, but the short re-forecast period made more elaborate trend

367 computations hazardous.

368

369 **3.2 Pan-Arctic sea ice extent skill**

370

371 As a first glimpse of the skill of different systems in re-forecasting sea ice conditions, we focus on
372 Pan-Arctic sea ice extent RMSE and correlation over the 1993-2014 re-forecast period are shown in
373 Fig. 3, and results for September summarized in Table 2.

374

375 The skill of individual systems is compared to a multi-model ensemble (MME) grouping all ensemble
376 members of each system together (without weighting individual systems but with equal weight for
377 each member). The skill of the MME is shown in black. Scores can be compared to a simple
378 persistence approach (persisting SIE anomalies from April to the following months) for which results
379 are shown in magenta. Most systems exhibit fairly similar levels of skill, both for RMSE and
380 correlation. RMSE is maximum in September when SIE is at the minimum of the seasonal cycle.
381 Correlation drops (as expected) with lead time, from above 0.8 in May to near-zero correlation for
382 two of the models in October, namely CNRM-CM6-1 and EC-Earth 3.2, although in the case of the
383 latter, this may be due to the smaller ensemble size. The three operational systems generally exhibit
384 significant levels of correlation with NSIDC data at a 6-month lead time, although MF-Sys6 drops
385 below the 95% significance threshold for August and September SIE (see Table 2 for September
386 RMSE and correlation values). As expected from the results of the individual models, the C3S-MME
387 (in orange) outperforms the MME for both metrics in the long forecast times. All models show higher
388 skill than persistence, although the score for persistence is included inside the range of uncertainty of
389 the scores (based on a χ^2 for RMS and a Fisher test for correlation) after 2 months forecast time in
390 most cases (not shown). This is likely related to the limited number of re-forecast years in the
391 evaluation.

392

393 Although not strictly comparable due to different re-forecast years, the results found for SIE
394 correlation and RMSE are consistent with previous works: Wang et al. (2013) and Msadek et al.
395 (2014) found similar performances with other re-forecast systems in terms of SIE correlation. Msadek
396 et al. (2014) also showed evidence that skill tends to be lower in recent decades than over a longer re-
397 forecast period spanning also the 1980s. More recently, Bushuk et al. (2019) showed with the GFDL-
398 FLOR model a sharp drop in summer pan-Arctic SIE anomaly correlation for May initializations as
399 early as June (see their Fig. 5).

400

401 **3.3 Sea ice edge forecast quality**

402

403 While seasonal forecasts of Pan-Arctic sea ice can provide some indication of below-average or
404 above-average presence of sea ice, these may not be the most relevant indicators for potential end-
405 users of seasonal forecast information. Among these users, some are most interested in the exact
406 position of the sea ice edge, or its probability of presence along shipping routes or near the
407 climatological sea ice edge (Melia et al. 2017).

408

409 We therefore evaluate the skill of the different models in representing the position of the sea ice edge
410 (based on monthly averages) by computing the IIEE metric introduced by Goessling et al. (2016).
411 This is first done after correcting SIC for systematic errors with a simple cross-validation bias
412 removal.

413

414 Figure 4 shows the IIEE for each individual model for September 1993-2014, as well as for the MME
415 and C3S-MME (after individual model bias correction). Results for the different models are quite
416 similar, with IIEE increasing during the re-forecast period, mainly due to an increase in AEE. This
417 positive trend in AEE is consistent with the models under-estimating the negative trend in SIE
418 discussed previously.

419

420 Peaks in IIEE are found in 2007 and 2012 for each system, indicating that all models missed to some
421 extent the record low SIE for both of these years. Conversely, in the first half of the re-forecast period,
422 most models exhibit their highest IIEE for 1996 for which SIE was the highest of the 1993-2014
423 period. IIEE is (by construction) very sensitive to errors in forecast extrema. These results can be
424 expected given the low predictability of such extrema, partly due to atmospheric conditions at
425 synoptic scales which are inherently unpredictable at such large forecast times. However, in the case
426 of the 2012 minimum, past studies using observational data and GCM experiments suggest that the
427 role of an extreme summer storm over the Arctic was minor compared to sea ice preconditioning and
428 warmer near-surface atmospheric temperature conditions during the summer season (Zhang et al.
429 2013, Guemas et al. 2013).

430

431 The operational systems show generally less variability in the misplacement error than CNRM-CM6-
432 1 and EC-Earth 3.2, apart from MF-Sys6 in the first half of the re-forecast period. This suggests that
433 for the former, skill evaluations based on RMSE of Pan-Arctic SIE are giving a rather accurate picture
434 of the model capacity to predict the sea ice edge position, whereas for the latter two systems, the Pan-
435 Arctic SIE may “hide” some compensation between areas where SIC is overestimated and where it is
436 underestimated.

437

438 For some systems, IIEE tends to grow during the re-forecast period, which may be related to the

439 strong decrease in total SIE during 1993-2014. We therefore re-compute the IIEE score after trend-
440 adjusting the SIC as described in section 2.2. Results are shown in Fig. 5. With this SIC trend
441 adjustment, the minimum over the period is 2007 (and 2012 no longer appears as a year with low
442 SIE). All models miss the 2007 anomaly with a large AEE. As found previously using SIC data
443 corrected for the mean bias, the AEE is the largest contribution (on average) for September IIEE in all
444 systems.

445

446 In order to evaluate the impact of trend-adjustment on IIEE, and also extend the analysis to the other
447 months of the re-forecasts, we show in Fig. 6 the mean evolution as a function of forecast time of the
448 IIEE in the different models and both MMEs considered, using bias-corrected SIC data (left) and
449 trend-adjusted SIC data (right). Trend adjustment does improve the mean IIEE values for most
450 systems, although some seem to benefit far more from this technique than others. For instance,
451 focusing again on the month of September, the CNRM-CM6-1 model forecasts are clearly improved,
452 whereas EC-Earth 3.2 and SEAS5 IIEE are only slightly reduced. It is also worth noticing in Fig. 6
453 that both the MME (in black) and C3S MME (in orange) exhibit very similar results in terms of IIEE,
454 and improve all the individual forecasts for almost every forecast month, irrespective of the bias
455 adjustment technique used. When compared to SIE RMSE values in Fig. 3, IIEE values (which are
456 dominated by the AEE term) exhibit substantially higher values. Although the computation method
457 for total sea ice extent differs between Fig. 3 and Figs. 5-6, this suggests that further improvements
458 would be found with more sophisticated bias correction and trend-adjustment techniques.

459

460 The IIEE peaks in September when the total SIE is lowest, and the opposite sign in the evolution of
461 average IIEE and SIE during summer is quite striking. Some models did seem to exhibit (to some
462 degree) a return of skill in terms of correlation and RMSE between September and October (see Fig.
463 3) which is also suggested by the decrease in IIEE.

464

465 Ensemble forecasts bear the advantage that information can be provided in probabilistic form to
466 potential users. This is most useful when the forecast is associated with a potential risk and
467 corresponding losses for the user, as different courses of action may be undertaken depending on a
468 given probability threshold, and at the time scales considered in this study, forecasts are rarely yes/no
469 answers as they bear intrinsic uncertainties. We therefore focus in the following paragraph on the
470 probabilistic extension of the IIEE, the SPS.

471

472 **3.4 Probabilistic re-forecasts of sea ice edge**

473

474 We compute the SPS using monthly SIC re-forecasts and a 15% SIC threshold for presence or
475 absence of sea ice, with two approaches to bias-adjust the model data over the re-forecast period. The

476 first method used is a grid-point bias correction of the probabilities for each model (or multi-model) to
477 exceed the 0.15 threshold, using leave-one-out cross-validation. Probabilities exceeding 1 or below 0
478 are readjusted to 1 or 0, respectively. The second method uses the same adjustment of probabilities,
479 but computes these after applying the trend adjustment to the SIC values. Figure 7 shows results
480 according to the forecast month for each individual model as well as the 5-model and C3S MMEs.
481 Consistent with deterministic results for the IIEE, the MMEs rank among the best models (low SPS)
482 for each forecast time with the first adjustment, and tend to outperform all the individual systems after
483 the second adjustment, but skill scores are not significantly better. Year-to-year values for SPS are not
484 shown, since very limited inter-annual variability in SPS is found - setting aside the 1996, 2007 or
485 2012 cases during which SIE over the Pan-Arctic region reached local extrema.

486

487 As found previously, the SIC trend adjustment technique helps further improve skill levels. This is
488 particularly striking in the case of the CNRM-CM6-1 model, which suffered from large systematic
489 errors in SIC at longer forecast times, and shows that despite these issues some predictive skill
490 remains.

491

492 In most cases, by comparing Fig. 7 with Fig. 6, it appears that the SPS values are clearly lower than
493 the corresponding IIEE. This suggests that in areas where uncertainty is high, the spread in the models
494 tends to reduce the probabilities for presence of sea ice, so models are generally not too
495 overconfident. These considerations prompted the analysis of model reliability shown in the following
496 section, which focuses on the skill at a regional level.

497

498 **4. Regional skill**

499

500 In this section we focus on skill of the different models over different key regions of the Arctic. Based
501 on previous results, we target our analysis on the IIEE for sub-basins, as well as the Brier Score and
502 reliability and resolution components to characterize probabilistic skill. Note that the SPS is a
503 spatially weighted Brier Score for the event of SIC exceeding the 0.15 threshold set in this study to
504 define the presence of sea ice. Our analysis focuses on the extended Beaufort-Chukchi Seas and
505 Laptev-East Siberian Seas sectors, as well as the Barents-Kara region, where all models exhibit strong
506 biases at forecast month 5.

507

508 Figure 8 shows the models and multi-models IIEE after trend-adjustment as a function of forecast
509 time over the Beaufort-Chukchi Seas (a), Laptev-East Siberian Seas (b), and the Barents and Kara
510 seas (c). For the Beaufort-Chukchi and Laptev-East Siberian seas, all models exhibit similar
511 evolutions with forecast time, quite similar to the total SIE over the region. As for the total Pan-Arctic

512 region, IIEE is maximum when the SIE is minimum, and then drops in October. May IIEE is close to
513 zero for each system, suggesting that models are correctly initialized as fully ice-covered over these
514 regions and error grows quite slowly initially. In the Laptev-East Siberian seas sector, the October
515 IIEE is very similar for all systems due to the annual cycle of sea ice extent over the region: only a
516 few years in NSIDC data show some ice-free areas in these seas, and they are generally not captured
517 by the different forecasting systems at such long forecast ranges (not shown). The MME and C3S
518 MME IIEE values nearly overlap (black and orange lines), indicating that the CNRM-CM6-1 and EC-
519 Earth 3 models do not necessarily provide additional value to the multi-model approach in these areas.
520 Skill is very limited compared to re-forecasts based on a simple linear trend climatology (Clim in Fig.
521 8), although more systems outperform this empirical forecast over the Beaufort-Chukchi sector than
522 over the Laptev-East Siberian seas.

523

524 Over the Barents and Kara sector, the IIEE evolution exhibits a quite different behavior. From the first
525 month of the re-forecasts, some errors in the ice edge are found in the different systems, leading to a
526 first peak of IIEE in July for which the IIEE amounts to almost half of the total SIE over the area.
527 However, the error of the linear trend climatology forecast is higher than each system from May to
528 July, and higher than most systems up to October. This suggests that although predictability of
529 summer sea ice over the Barents and Kara seas is very limited, dynamical systems do provide some
530 information on SIE beyond simple empirical forecasts.

531

532 We evaluate the probabilistic skill in forecasting the presence of ice by plotting reliability diagrams
533 for each region, alongside the Brier Skill Score (BSS) and reliability and resolution components of the
534 Brier Score for the event of SIC in the grid cell exceeding 0.15. The probabilistic forecasts are
535 evaluated after bias correcting or trend-adjusting the SIC data as previously described for the Pan-
536 Arctic SPS. Since over the 1993-2014 period, most of the Barents-Kara Seas region is ice-free in
537 September, we show results for the Beaufort-Chukchi and Laptev-East Siberian Seas regions only.
538 Results for the C3S operational re-forecasts and the C3S MME for September over the Beaufort-
539 Chukchi region are shown in Fig. 9. Comparing the top and bottom rows, we find that trend
540 adjustment improves the reliability and resolution of the forecasts. This translates into higher BSS for
541 each system. Unlike SEAS5 and GloSea5 (Fig. 9 e-f), MF-Sys6 (g) almost systematically
542 underestimates the probabilities of presence of ice, whereas the other systems tend to have too high
543 forecast probability values with respect to the observed occurrence of the event (SEAS5 more
544 dramatically so than GloSea5).

545

546 Over the Laptev and Siberian Seas (Fig. 10), trend adjustment noticeably improves the reliability of
547 all systems considered, with reliability diagrams closely fitting the perfect reliability diagonal. Out of
548 the three operational systems, MF-Sys6 is the one which is most improved after trend adjustment,

549 since using a simple bias correction led in this case to practically no skill over climatology in
550 predicting the presence of ice over the region. All systems (including the C3S MME) have very
551 similar levels of resolution after trend adjustment, demonstrating the interest of correcting for the
552 trend in sea ice concentration before formulating probabilistic forecasts for the presence of ice.

553

554

555

556 **5. Summary and discussion**

557

558 In this study, a comprehensive multi-system ensemble was evaluated for boreal summer predictions of
559 sea ice by grouping re-forecasts from three operational systems with two ensembles with current
560 generation GCMs (CNRM-CM6-1 and EC-Earth 3.2). The common re-forecast period, 1993-2014,
561 coincides with the highest trends in sea ice concentration and extent over the Pan-Arctic region. The
562 focus of this study was on sea ice concentration and extent, and using metrics designed to assess the
563 ability of models to represent the position of the sea ice edge. A companion study by Acosta Navarro
564 et al. (2020) examines the link in these models between fall Arctic sea ice and Northern Hemisphere
565 boreal winter atmospheric seasonal forecast skill.

566

567 Models exhibit diverse levels of forecast quality and ability to reproduce tendencies in sea ice extent
568 estimated with NSIDC data. Beyond this comparison, a multi-model approach either grouping all five
569 models or the three operational C3S systems does not lead to major improvements, especially with
570 respect to the best systems, besides reliability and resolution components when investigating
571 probabilistic skill over the Beaufort-Chukchi and Laptev-East Siberian seas. However, either the
572 MME or C3S MME rank systematically among the two best models at all lead times and cases
573 examined, which pleads in favor of model diversity, and is consistent with pan-Arctic and regional
574 evaluations of probabilistic skill of single-models and multi-models discussed in Dirkson et al.
575 (2019a). Yet some model deficiencies leading to strong biases or errors in trends do seem to alter the
576 MME skill. This highlights the need for a careful bias correction and trend adjustment of current state-
577 of-the-art forecasting systems, as a necessary first step before using such predictions. These results
578 confirm the limited predictability of summer Arctic sea ice with current state-of-the-art GCMs,
579 especially at longer forecast times such as five months ahead of the September sea ice minimum.
580 They are consistent with recent results suggesting a “spring predictability barrier” in prediction skill
581 (e.g. Bonan et al. 2019).

582

583 One major limitation to statistical post-processing and adjustments of forecasts is the very restricted
584 number of years available for the evaluation of seasonal forecast biases and skill. The use of linear
585 trends over longer time periods may quickly show some limitations, especially with bounded

586 variables such as sea ice concentration. Director et al. (2017) emphasized the limitations related to
587 such bias correction techniques which can lead to unrealistic sea ice edges, and designed a contour
588 shifting method which corrects using linear regression the position of the sea ice edge. Dirkson et al.
589 (2019b) found additional improvements in terms of probabilistic skill scores when fitting the sea ice
590 concentration distribution to a parametric distribution and applying a trend-adjusted quantile mapping
591 correction. These methods would likely further enhance skill scores of the systems evaluated in this
592 study. However, given the coarse common spatial resolution used, the restricted number of re-forecast
593 years, and the same statistical treatment applied to our benchmark forecasts, we are confident the bias
594 and trend adjustment applied yield results that are representative of the actual capacity of these
595 models to forecast summer Arctic sea ice over simple empirical approaches. Another source of
596 possible error in the estimation of skill levels is the reference data used. The NSIDC data is known to
597 have some uncertainties, in particular during the summer season where melt ponds can be interpreted
598 as ice free areas, but was chosen so as to provide a fair comparison between systems (since none were
599 initialized directly from this dataset).

600

601 The diverse levels of skill likely arise from differences in the sea ice initialization and modeling
602 strategies, as suggested by recent works on the S2S scale by Zampieri et al. (2018) and Wayand et al.
603 (2019). In particular, the results found for re-forecasts based on CNRM-CM (either CNRM-CM6-1 or
604 MF-Sys6) show substantially lower skill than in previous studies (e.g. Chevallier et al. 2013).
605 Ongoing evaluation of these systems show that they exhibit from the first month of the re-forecasts
606 lower sea ice thickness than reference datasets. The initialization of sea ice thickness has been
607 identified by recent works as a source of predictability on seasonal time scales, either by direct
608 assimilation (Blockley et al., 2018) or constraining SIT with SIC (Kimmritz et al., 2019). Other
609 important processes for the melt season, such as melt ponds, are still only partially represented in
610 models used in this study. Some pathways for improvement of current systems are currently explored
611 in the framework of the APPLICATE project and will hopefully contribute to better and more robust
612 forecasts of Arctic sea ice at the seasonal time scale in years to come.

613

614 **Acknowledgements and data**

615

616 This study was partly funded by the H2020-APPLICATE project, EU grant number 727862.
617 Copernicus C3S seasonal re-forecast data for ECMWF SEAS5, Met Office GloSea5 and Météo-
618 France System 6 were retrieved using the Mars API. The reforecasts with the EC-Earth 3.2 and
619 CNRM-CM6-1 models were run as part of the H2020-APPLICATE project and data is available on
620 the APPLICATE data portal or upon request.

621 JCAN acknowledges the Spanish Ministry of Science, Innovation and Universities for the personal

622 grant Juan de la Cierva FJCI-2017-34027, PRACE for awarding access to MareNostrum at Barcelona
623 Supercomputing Center (BSC), and ESA/CMUG-CCI3 for financial support. PO work was funded by
624 the Ramon y Cajal grant RYC-2017-22772.

625 The authors wish to acknowledge F. Massonnet who developed the sea ice assimilation technique
626 used to initialize EC-Earth 3.2, and S. Tietsche for pointing to the relevant SEAS5 data.

627 All plots and graphs were realized using R, and some skill evaluations and data detrending were
628 computed using the s2dverification package available on CRAN (Manubens et al. 2018).

629 The authors would also like to thank two anonymous reviewers, whose feedback helped substantially
630 improve this article.

631

632 This is a post-peer-review, pre-copyedit version of an article published in Climate Dynamics. The
633 final authenticated version is available online at: <http://dx.doi.org/10.1007/s00382-020-05273-8>

634 **References**

635

636 Acosta-Navarro, J. C., P. Ortega, L. Batté, D. Smith, P.-A. Bretonnière, V. Guemas et al. (2020) Link
637 between autumnal Arctic Sea ice and Northern Hemisphere winter forecast skill, *Geophys. Res. Lett.*,
638 accepted.

639

640 Balmaseda, M. A., K. Mogensen, and A. T. Weaver (2013) Evaluation of the ECMWF ocean
641 reanalysis system ORAS4, *Q. J. Roy. Meteor. Soc.*, 139, 1132–1161, doi: 10.1002/qj.2063

642

643 Batté, L. and M. Déqué (2016) Randomly correcting model errors in the ARPEGE-Climate v6. 1
644 component of CNRM-CM: applications for seasonal forecasts, *Geosc. Mod. Dev.* 9 (6), doi:
645 10.5194/gmd-9-2055-2016.

646

647 Blackport, R., J. A. Screen, K. van der Wiel and R. Bintanja (2019) Minimal influence of reduced
648 Arctic sea ice on coincident cold winters in mid-latitudes. *Nature Climate Change*, [9\(9\), 697-704](#).

649

650 Blanchard-Wrigglesworth, E., K. C. Armour, C. M. Bitz and E. DeWeaver (2011) Persistence and
651 inherent predictability of Arctic sea ice in a GCM ensemble and observations, *J. Clim.* 24: 231–250.

652

653 Blanchard-Wrigglesworth, E., A. Barthélemy, M. Chevallier, R. Cullather, N. S. Fuckar et al. (2017)
654 Multi-model seasonal forecast of Arctic sea-ice: forecast uncertainty at pan-Arctic and regional scales.
655 *Clim. Dyn.*, doi:10.1007/s00382-016-3388-9

656

657 Blockley, E. W. and K. A. Peterson (2018). Improving Met Office seasonal predictions of Arctic sea
658 ice using assimilation of CryoSat-2 thickness. *The Cryosphere*, 12, 3419–3438. doi:10.5194/tc-12-
659 3419-2018

660

661 Bonan, D. B., M. Bushuk, and M. Winton (2019). A spring barrier for regional predictions of summer
662 Arctic sea ice. *Geophys. Res. Lett.* 46, 5937–5947. doi:10.1029/2019GL082947

663

664 Brodeau, L., Barnier, B., Treguier, A. M., Penduff, T., & Gulev, S. (2010). An ERA40-based
665 atmospheric forcing for global ocean circulation models. *Ocean Modelling*, 31(3-4), 88-104.

666

667 Bushuk, M. et al. (2017) Skillful regional prediction of Arctic sea ice on seasonal timescales.
668 *Geophys. Res. Lett.* 44, 4953–4964, doi:10.1002/2017GL073155

669

670 Bushuk, M., R. Msadek, M. Winton, G. Vecchi et al. (2019) Regional Arctic sea–ice prediction:

671 potential versus operational seasonal forecast skill. *Clim. Dyn.*, [52 \(5-6\), 2721-2743](#), doi:
672 10.1007/s00382-018-4288-y

673

674 Cavalieri, D.J., C.L. Parkinson, P. Gloersen and H.J. Zwally (1996, updated yearly). Sea ice
675 concentrations from Nimbus-7 SMMR and DMSP SSM/I-SSMIS passive microwave data, version 1.
676 Boulder, Colorado USA. *NASA National Snow and Ice Data Center Distributed Active Archive*
677 *Center*. doi: 10.5067/8GQ8LZQVL0VL. (Accessed 20 February 2017)

678

679 Chevallier, M. and D. Salas y Mélia (2012). The role of sea ice thickness distribution in the Arctic sea
680 ice potential predictability: A diagnostic approach with a coupled GCM. *J. Clim.* 25: 3025–3038.

681

682 Chevallier, M., D. Salas y Mélia, A. Voldoire, M. Déqué, and G. Garric (2013). Seasonal forecasts of
683 the pan-Arctic sea ice extent using a GCM-based seasonal prediction system. *J. Clim.* [26\(16\): 6092-](#)
684 [6104](#), doi: 10.1175/JCLI-D-12-00612.1.

685

686 Chevallier, M., G.C. Smith, F. Dupont et al. (2017). Intercomparison of the Arctic sea ice cover in
687 global ocean–sea ice reanalyses from the ORA-IP project. *Clim Dyn* 49: 1107, doi: 10.1007/s00382-
688 016-2985-y

689

690 Coumou, D., G. Di Capua, S. Vavrus, L. Wang and S. Wang (2018) The influence of Arctic
691 amplification on mid-latitude summer circulation. *Nature Comm.* 9, 2959, doi: 10.1038/s41467-018-
692 05256-8

693

694 Cruz-Garcia, R., V. Guemas, M. Chevallier and F. Massonnet (2019) An assessment of regional sea
695 ice predictability in the Arctic ocean. *Clim. Dyn.*, doi: 10.1007/s00382-018-4592-6, *in press*.

696

697 Day, J.J., S. Tietsche and E. Hawkins (2014) Pan-Arctic and Regional Sea Ice Predictability:
698 Initialization Month Dependence. *J. Clim.* 27: 4371–4390, doi: 10.1175/JCLI-D-13-00614.1.

699

700 Director, H. M., A. E. Raftery and C. M. Bitz (2017) Improved Sea Ice Forecasting through
701 Spatiotemporal Bias Correction. *J. Clim.*, 30, 9493-9510, doi:10.1175/JCLI-D-17-0185.1

702

703 Dirkson, A., B. Denis, and W. J. Merryfield (2019a) A multimodel approach for improving seasonal
704 probabilistic forecasts of regional Arctic sea ice. *Geophys. Res. Lett.*, 46, 10,844–10,853,
705 doi:10.1029/2019GL083831

706

707 Dirkson, A., W. J. Merryfield and A. H. Monahan (2019b) Calibrated probabilistic forecasts of Arctic

708 sea ice concentration. *J. Clim.*, 32, 1251-1271, doi:10.1175/JCLI-D-18-0224.1
709

710 Eicken, H. (2013) Arctic sea ice needs better forecasts. *Nature* **497**, 431–433, doi:10.1038/497431a
711

712 Ferry, N., Parent, L., Garric, G., Barnier, B., et al. (2010), ‘Mercator global Eddy permitting ocean
713 reanalysis GLORYS1V1 : Description and results’, Mercator-Ocean Quarterly Newsletter 36, 15–27.
714 [https://www.mercator-ocean.fr/sciences-publications/mercator-ocean-journal/newsletter-36-data-](https://www.mercator-ocean.fr/sciences-publications/mercator-ocean-journal/newsletter-36-data-assimilation-and-its-application-to-ocean-reanalyses/)
715 [assimilation-and-its-application-to-ocean-reanalyses/](https://www.mercator-ocean.fr/sciences-publications/mercator-ocean-journal/newsletter-36-data-assimilation-and-its-application-to-ocean-reanalyses/)
716

717 Fichefet, T. and M. A. Maqueda (1997) Sensitivity of a global sea ice model to the treatment of ice
718 thermodynamics and dynamics, *J. Geophys. Res.-Oceans*, 102, 12609–12646, doi:
719 10.1029/97JC00480
720

721 Francis, J. A., N. Skific, S. J. Vavrus (2018) North American Weather Regimes Are Becoming More
722 Persistent: Is Arctic Amplification a Factor? *Geophys. Res. Lett.* 45, 11,414-11,422,
723 doi:10.1029/2018GL080252
724

725 García-Serrano, J., et al. (2015) On the predictability of the winter Euro-Atlantic climate: lagged
726 influence of autumn Arctic sea ice. *Journal of Climate* 28 (13): 5195-5216.
727

728 Germe, A., M. Chevallier, D. Salas y Mélia, E. Sanchez-Gomez and C. Cassou (2014) Interannual
729 predictability of Arctic sea ice in a global climate model: regional contrasts and temporal evolution.
730 *Climate Dynamics*, **43** (9-10), 2519-2538, doi: 10.1007/s00382-014-2071-2
731

732 Goessling, H.F. et al. (2016) Predictability of the Arctic sea ice edge. *Geophys. Res. Lett.* 43, 1642-
733 1650, doi:10.1002/2015GL067232
734

735 Goessling, H.F. and T. Jung (2018) A probabilistic verification score for contours: Methodology and
736 application to Arctic ice-edge forecasts. *Q. J. R. Meteorol. Soc.*, doi:10.1002/qj.3242, *in press*.
737

738 Guemas V., F. Doblas-Reyes, A. Germe, M. Chevallier and D. Salas y Mélia (2013) September 2012
739 Arctic sea ice minimum : Discriminating between sea ice memory, the August 2012 extreme storm
740 and prevailing warm conditions [in "Explaining Extreme Events of 2012 from a Climate
741 Perspective"], *Bull. Amer. Meteor. Soc.*, 94 (9), S20-S22, doi: 10.1175/BAMS-D-13-00085.1
742

743 Guemas, V., E. Blanchard-Wrigglesworth, M. Chevallier, J. J. Day, M. Déqué et al. (2016) A review
744 on Arctic sea-ice predictability and prediction on seasonal to decadal time-scales. *Q. J. R. Meteorol.*

745 Soc. 142: 546-561, doi: 10.1002/qj.2401
746
747 Hagedorn, R., F.J. Doblas-Reyes and T.N. Palmer (2005) The rationale behind the success of multi-
748 model ensembles in seasonal forecasting - I. Basic concept. *Tellus A: Dynamic Meteorology and*
749 *Oceanography*, 57A, 219-233, doi: 10.3402/tellusa.v57i3.14657
750
751 Johnson, S., T. N. Stockdale, L. Ferranti, M. A. Balmaseda, F. Molteni et al. (2019) SEAS5: the new
752 ECMWF seasonal forecast system. *Geosci. Model Dev.*, 12, 1087–1117, doi: 10.5194/gmd-12-1087-
753 2019
754
755 Jung, T., et al. (2015) Polar lower-latitude linkages and their role in weather and climate prediction.
756 *Bull. Amer. Meteor. Soc.*, **96**, ES197–ES200, doi: [10.1175/BAMS-D-15-00121.1](https://doi.org/10.1175/BAMS-D-15-00121.1).
757
758 Kimmritz, M., F. Counillon, L. H., I. Bethke, N. Keenlyside, F. Ogawa and Y. Wang (2019) Impact of
759 ocean and sea ice initialisation on seasonal prediction skill in the Arctic. *J. Adv. Model. Earth Sy.*, 11,
760 4147–4166. doi:10.1029/2019MS001825
761
762 MacLachlan, C., A. Arribas, K. A. Peterson, A. Maidens, D. Fereday, A. A. Scaife, M. Gordon, M.
763 Vellinga, A. Williams, R. E. Comer, J. Camp, P. Xavier and G. Madec (2015) Global Seasonal
764 forecast system version 5 (GloSea5): a high-resolution seasonal forecast system. *Q. J. R. Meteorol.*
765 *Soc.*, 141, 1072-1084, doi:10.1002/qj.2396
766
767 Madec G., R. Bourdallé-Badie, P.-A. Bouttier et al (2017) NEMO ocean engine. doi:
768 10.5281/ZENODO.1472492
769
770 Manubens, N., L.-P. Caron, A. Hunter, O. Bellprat, E. Exarchou et al. (2018) An R package for
771 climate forecast verification. *Env. Mod. Soft.*, 103, 29-42, doi: 10.1016/j.envsoft.2018.01.018
772
773 Massonnet, F., H. Goosse, T. Fichefet and F. Counillon (2014), Calibration of sea ice dynamic
774 parameters in an ocean-sea ice model using an ensemble Kalman filter, *J. Geophys. Res. Oceans*, 119,
775 4168–4184, doi:10.1002/2013JC009705
776
777 Melia N., K. Haines, E. Hawkins and J. J. Day (2017) Towards seasonal Arctic shipping route
778 predictions. *Environ. Res. Lett.*, 12, 084005, doi: 10.1088/1748_9326/aa7a60
779
780 Merryfield, W. J., W.-S. Lee, W. Wang, M. Chen and A. Kumar (2013) Multi-system seasonal
781 predictions of Arctic sea ice. *Geophys. Res. Lett.*, 40 (8), 1551-1556, doi: 10.1002/grl.50317.

782

783 Msadek, R., G. A. Vecchi, M. Winton and R. G. Gudgel (2014) Importance of initial conditions in
784 seasonal predictions of Arctic sea ice extent. *Geophys. Res. Lett.*, 41, 5208–5215,
785 doi:10.1002/2014GL060799.

786

787 Olonscheck, D., T. Mauritsen and D. Notz (2019) Arctic sea-ice variability is primarily driven by
788 atmospheric temperature fluctuations. *Nature Geoscience*, 12: 430–434, doi: 10.1038/s41561-019-
789 0363-1.

790

791 Serreze, M. C. and J. Stroeve (2015) Arctic sea ice trends, variability and implications for seasonal ice
792 forecasting. *Phil. Trans. R. Soc. A*, 373: 20140159. doi:10.1098/rsta.2014.0159.

793

794 Tietsche, S., J.J. Day, V. Guemas, W. J. Hurlin, S.P.E. Keeley et al. (2014) Seasonal to interannual
795 Arctic sea ice predictability in current global climate models. *Geophys. Res. Lett.*, [41, 1035-1043](#), doi:
796 10.1002/2013GL058755.

797

798 Vancoppenolle, M., T. Fichefet, H. Goosse, S. Bouillon, G. Madec, and M.A. Morales Maqueda
799 (2009) Simulating the mass balance and salinity of Arctic and Antarctic sea ice. 1. Model description
800 and validation. *Ocean Modelling*, 27, 33-53, [doi : 10.1016/j.oceanmod.2008.10.005](#).

801

802 Vihma, T. (2014) Effects of Arctic sea ice decline on weather and climate: a review. *Surv. Geophys.*
803 **35**, 1175–1214.

804

805 Voldoire, A., D. Saint-Martin, S. Sénési, B. Decharme, A. Alias et al. (2019) Evaluation of CMIP6
806 DECK experiments with CNRM-CM6-1 *J. Adv. Model. Earth Sy.*, doi:10.1029/2019MS001683, *in*
807 *press*.

808

809 Walsh J. E., J. S. Stuart and F. Fetterer (2019) Benchmark seasonal prediction skill estimates based
810 on regional indices. *The Cryosphere*, 13, 1073–1088, doi:10.5194/tc-13-1073-2019

811

812 Wayand N. E., C. M. Bitz and E. Blanchard-Wrigglesworth (2019) A year-round subseasonal-to-
813 seasonal sea ice prediction portal. *Geophys. Res. Lett.*, 46, doi: 10.1029/2018GL081565, *in press*.

814

815 Weisheimer A., and T. N. Palmer (2014) On the reliability of seasonal climate forecasts. *J. R. Soc.*
816 *Interface*, 11: 20131162. doi:10.1098/rsif.2013.1162

817

818 Zhang J., R. Lindsay, A. Schweiger, and M. Steele (2013), The impact of an intense summer cyclone

819 on 2012 Arctic sea ice retreat, *Geophys. Res. Lett.*, 40, doi:10.1002/grl.50190.

820

821 Zuo, H., M. A. Balmaseda, S. Tietsche, K. Mogensen, and M. Mayer (2019): The ECMWF
822 operational ensemble reanalysis-analysis system for ocean and sea-ice: a description of the system and
823 assessment, *Ocean Sci.*, 15, 779–808, doi:10.5194/os-15-779-2019

824

825

826 **Tables**

827

828 **Table 1:** Characteristics of the seasonal re-forecasts evaluated. All systems are initialized with ERA-

829 Interim for the atmosphere component.

Model/System	CNRM-CM6-1	EC-Earth 3.2.2	SEAS5	GloSea5	MF-Sys6
Atmosphere	Arpege 6.3	IFS Cy36r4	IFS Cy43r1	UM v6	Arpege 6.2
Ocean	NEMO 3.6	NEMO 3.6	NEMO 3.4	NEMO 3.4	NEMO 3.6
Sea ice	Gelato v6	LIM3	LIM2	CICE 4.1	Gelato v6
Atmospheric resolution	~1.4° 91 levels	~0.7° 91 levels	36 km 91 levels	~0.7° 85 levels	~0.5° 91 levels
Ocean/ice resolution	1° 75 levels	1° 75 levels	0.25° 75 levels	0.25° 75 levels	1° 75 levels
Sea ice initial conditions	Gelato-NEMO run constrained towards Glorys 2V4 (Mercator)	Forced LIM3-NEMO run with ENKF SIC assimilation	ORA-S5	NEMOVAR	Gelato-NEMO run constrained towards Glorys 2V4 (Mercator)
Ensemble size	30	10	25	28*	25*

830 ** All re-forecasts are initialized on the 1st of the month, except for GloSea5 for which 7 members*831 *from the 9th, 17th and 25th of April as well as 7 from the 1st of May are grouped into a 28-member*832 *ensemble, and MF-Sys6 for which 12 members from the 20th and 25th of April are grouped with one*833 *member from the 1st of May into a 25-member ensemble.*

834

835

836 **Table 2:** Linear trend of SIE and RMSE of SIE after linear detrending (in thousands of km²/year) and
 837 correlation over 1993-2014 for September over the Pan Arctic region in the different models studied,
 838 the MME and C3S MME. Scores are computed against NSIDC SIC data.

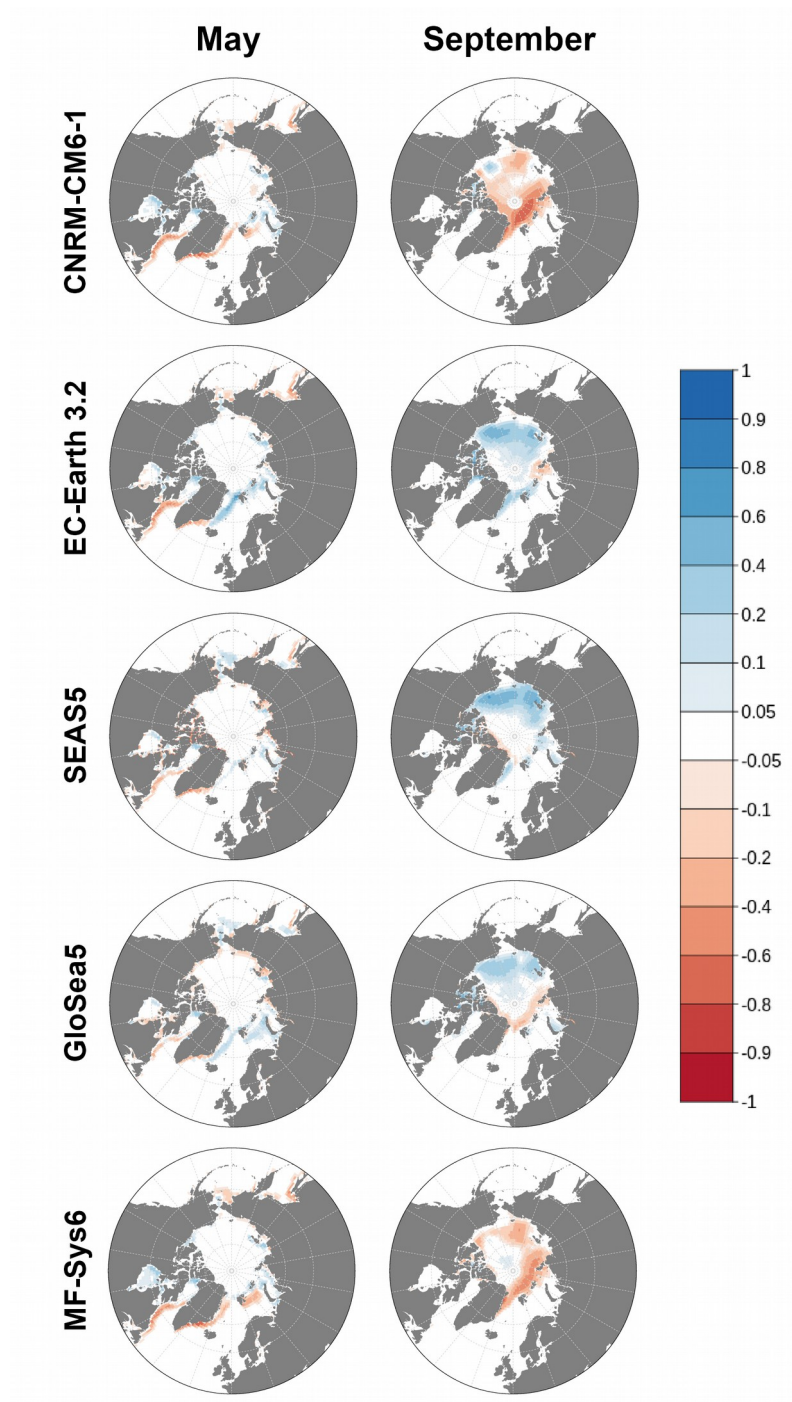
Model	CNRM- CM6-1	EC-Earth 3.2.2	SEAS 5	GloSea5	MF- Sys6	MME	C3S MME	Referen ce*
Sept. SIE linear trend	-84.1	-84.7	-44.0	-83.2	-95.9	-78.0	-74.7	-130.1
Sept. SIE RMSE	2443.6	666.0	957.1	625.4	2472.5	1208. 6	902.8	947.7
Sept. SIE RMSE (detrended)	702.4	595.8	543.8	535.9	584.3	570.2	543.1	693.7
Sept. SIE Correlation	0.66	0.78	0.79	0.84	0.80	0.81	0.83	0.34
Sept. SIE Correlation (detrended)	-0.09	0.15	0.35	0.38	0.17	0.21	0.35	-0.25

839 * Reference scores (RMSE, correlation) are computed for the persistence of April NSIDC SIE
 840 anomalies (magenta lines in Fig. 3). Reference trend is computed with NSIDC data.

841

842 Figures

843

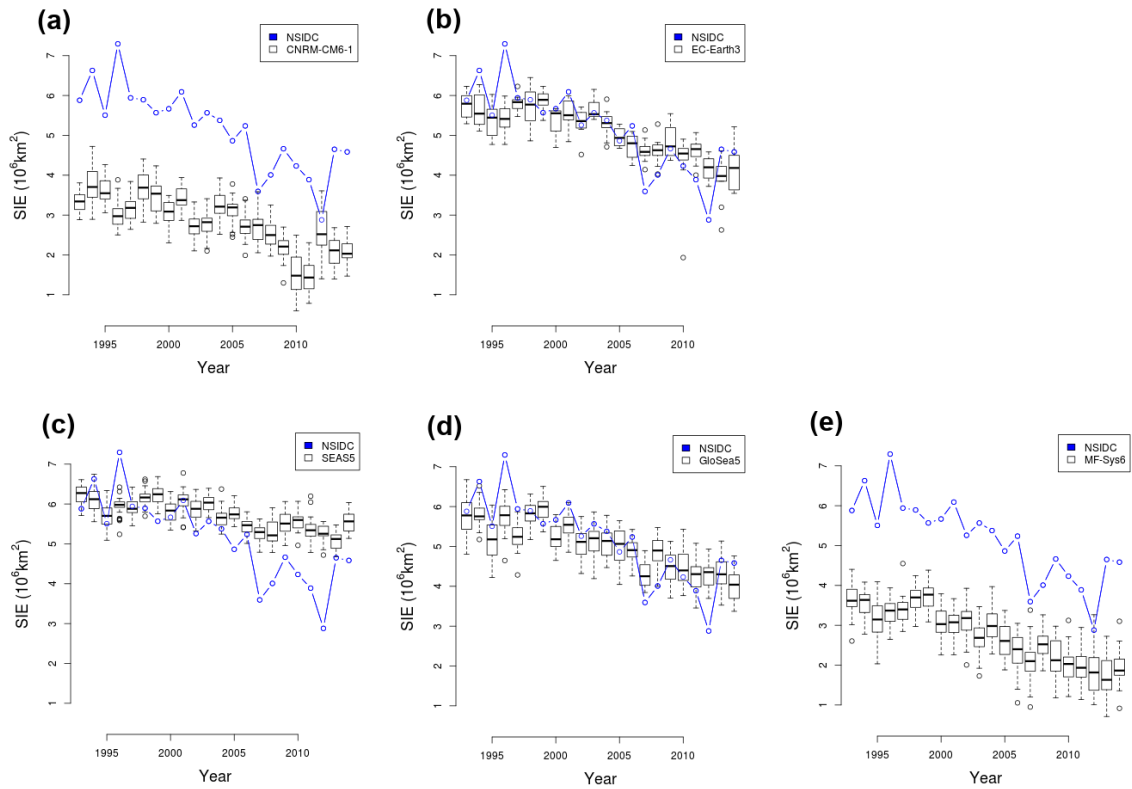


845

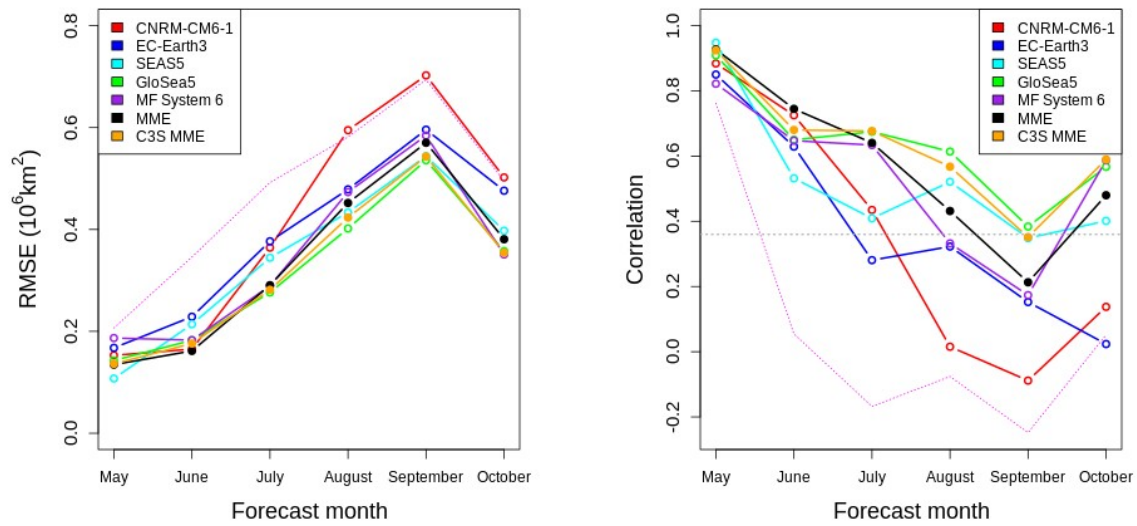
846 **Fig. 1** Mean bias in monthly mean sea ice concentration with NSIDC in May (forecast month 1, left

847 column) and September (forecast month 5, right column) for each of the coupled systems

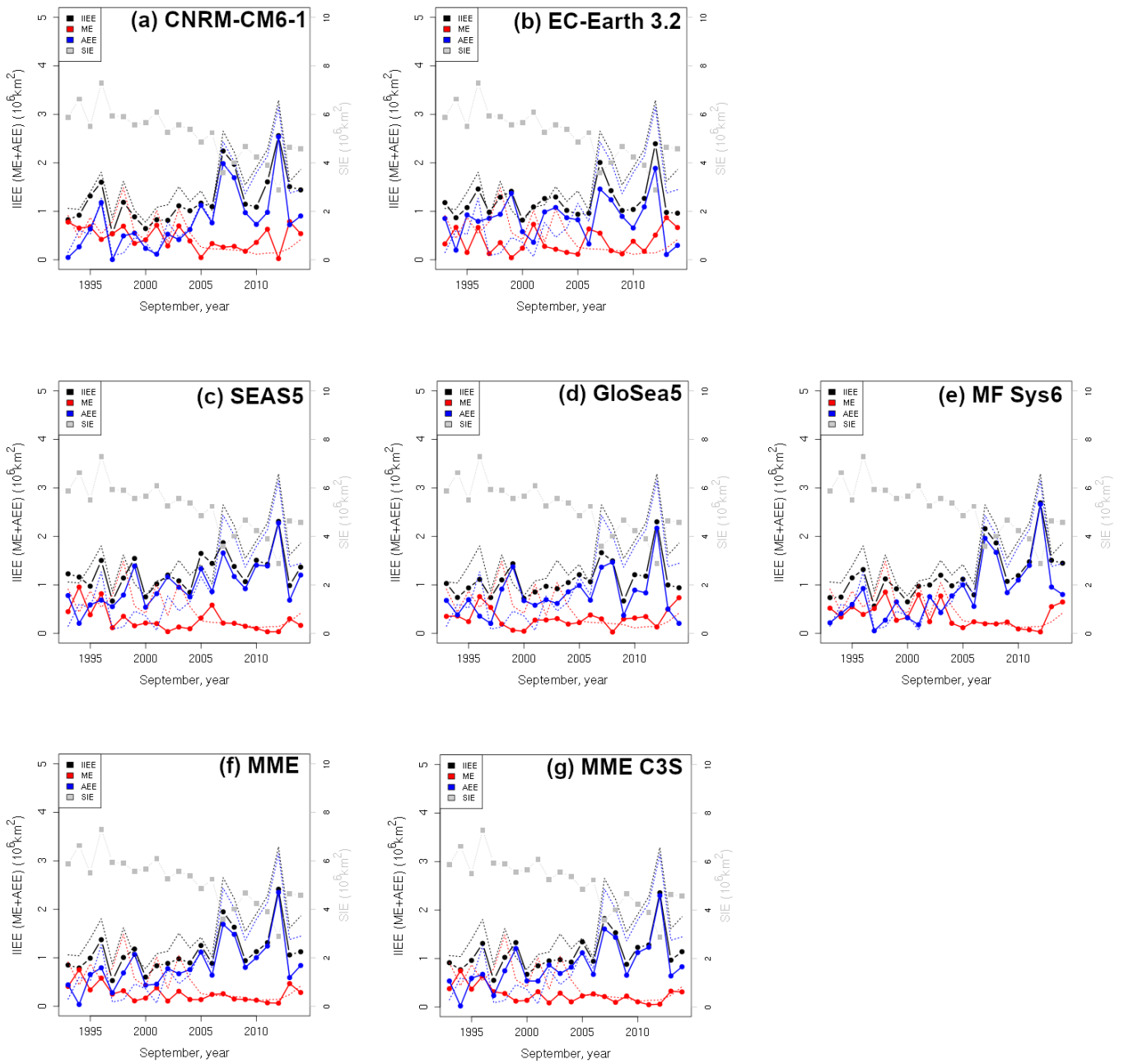
848



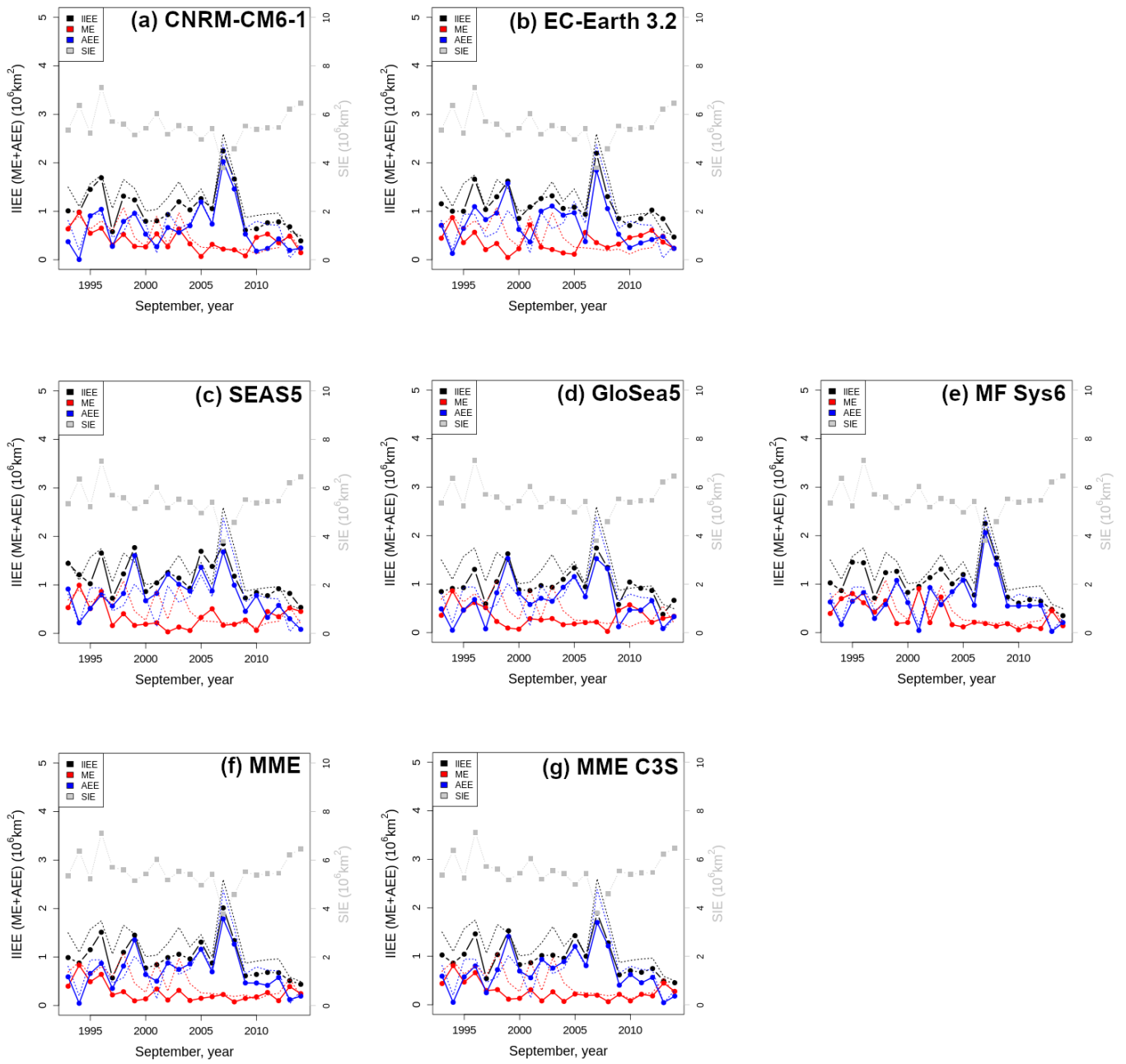
850 **Fig. 2** Box-and-whisker plots representing September SIE values for the re-forecast ensembles in each
 851 of the models (a) CNRM-CM6-1, (b) EC-Earth 3.2, (c) SEAS5, (d) GloSea5 and (e) MF-Sys6
 852 compared to NSIDC data (in blue). The boxes show the interquartile range of the ensembles, the thick
 853 black line is the ensemble median, and whiskers show the range of the ensemble up to 1.5σ , and dots
 854 represent outliers beyond this range
 855



857 **Fig. 3** Evolution according to forecast month of detrended pan-Arctic SIE RMSE (left) and
 858 correlation (right) with NSIDC reference data for the individual models (colored lines, open circles)
 859 and multi-model ensembles (filled circles). The multi-model ensemble (MME) is shown in black and
 860 the C3S MME in orange. Skill levels of the persistence of April anomalies are shown with a thin
 861 dotted magenta line. For correlation (right), a thin grey dotted line shows the 95% confidence
 862 threshold (0.36) computed using a one-sided t-test accounting for observational dependence of
 863 samples
 864

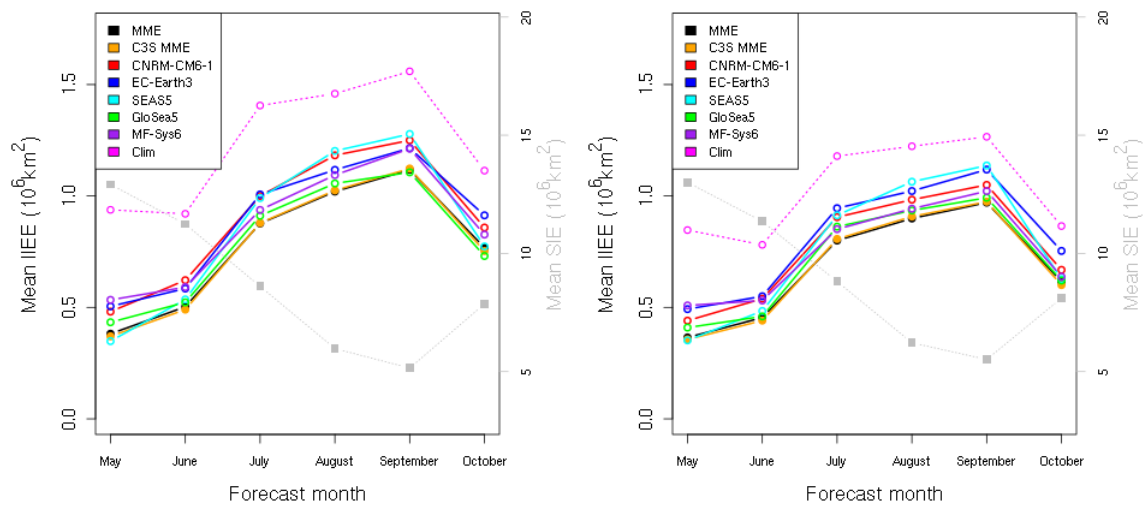


866 **Fig. 4** IIEE (black, in millions of km²) and decomposition in ME (red) and AEE (blue) with respect to
 867 NSIDC data for September 1993 to 2014 in re-forecasts initialized in May with (a) CNRM-CM6-1,
 868 (b) EC-Earth 3.2, (c) SEAS5, (d) GloSea5 and (e) MF-Sys6. (f) Same as (a-e) but for a multi-model
 869 ensemble grouping all ensemble members of each individual system (after individual bias correction
 870 of SIC). (g) Same as (f) but for the C3S operational systems (c-e). In each graph, thin dashed lines
 871 show the corresponding IIEE, ME and AEE values for a leave-one-out climatology based on NSIDC
 872 data, and the grey line shows the reference SIE (y-axis on the right hand side)



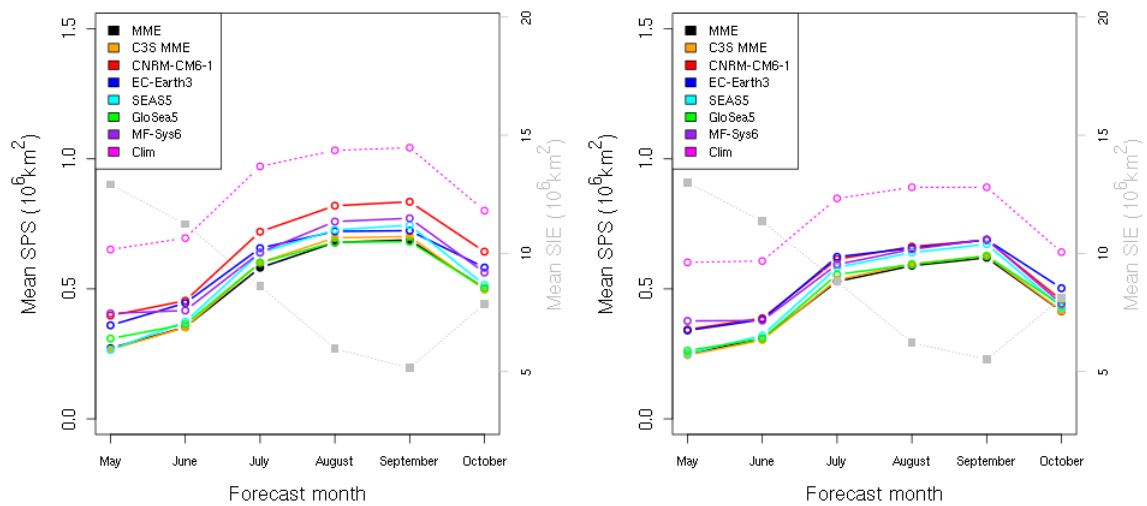
875 **Fig. 5** Same as Fig 4 but for IIEE computed after trend-adjusting SIC data at the gridpoint level. The
 876 dashed lines (IIEE, ME and AEE values of a forecast based on climatology) and SIE shown in grey
 877 are also computed from trend-adjusted SIC NSIDC data

878

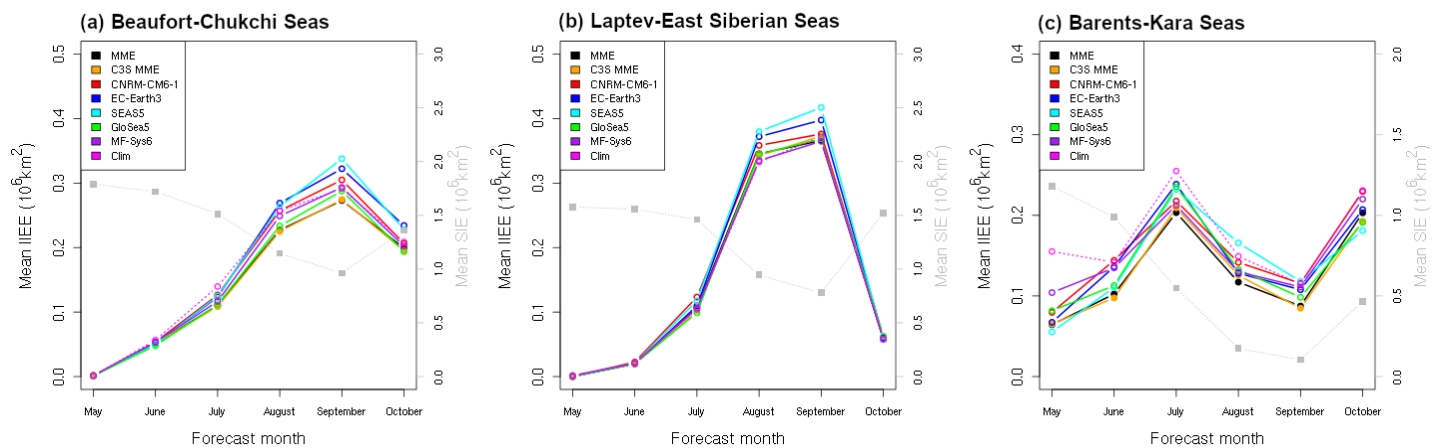


880 **Fig. 6** Evolution according to forecast time of mean IIEE computed using bias-corrected SIC data
 881 (left) and trend-adjusted SIC data (right) over the 1993-2014 re-forecast period for each model and the
 882 MME (in black) and C3S MME (in orange). Mean IIEE of the climatology forecasts (respectively,
 883 leave-one-out and trend-adjusted climatologies using NSIDC SIC data) are also shown (Clim, dotted
 884 magenta line). The monthly mean average SIE over 1993-2014 is shown in grey dotted lines (right y-
 885 axis)

886



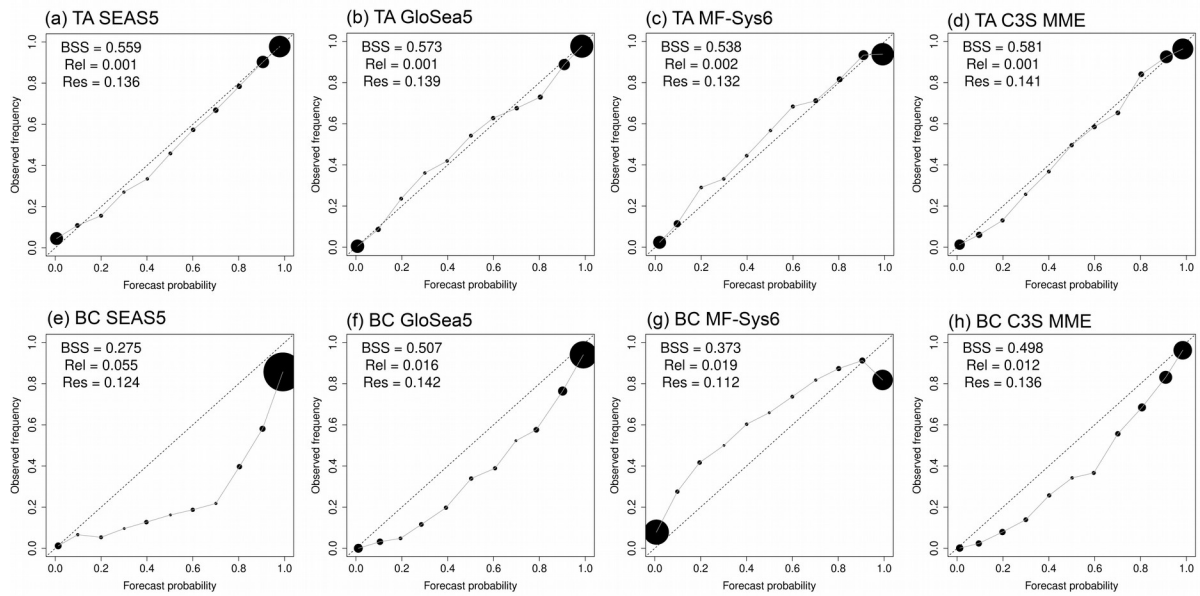
888 **Fig. 7** Left: mean SPS over 1993-2014 according to forecast month for each system and the MME (in
 889 black) and C3S MME (in orange), and 1993-2014 monthly mean SIE computed with NSIDC SIC data
 890 (in grey dotted line, right y-axis). SPS is computed after bias-correcting the probabilities of SIC
 891 exceeding 0.15. The benchmark forecast (Clim, in magenta) is based on a leave-one-out probability
 892 forecast using the other years of the 1993-2014 period. Right: same as left-hand-side figure but after
 893 additionally trend-adjusting SIC values before computing probabilities; the Clim forecast is in this
 894 case a linear trend adjusted leave-one-out probability forecast.
 895
 896



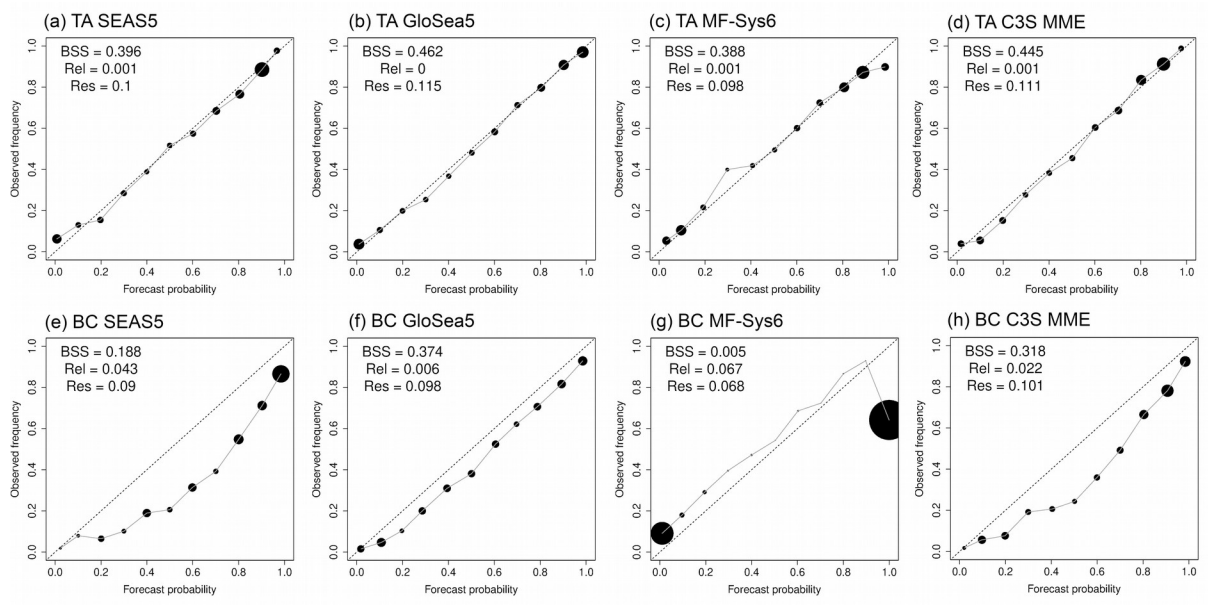
898 **Fig. 8** IIEE computed for trend-adjusted SIC re-forecasts for each model and the 5-model and C3S
 899 MME, over the extended Beaufort-Chukchi Seas region (a), the extended Laptev-East Siberian Seas
 900 region (b) and the Barents-Kara Seas region (c). IIEE for a benchmark climatology forecast based on
 901 linear trend-adjusted SIC is also plotted (in magenta dashed lines). Total SIE over the regions are
 902 shown in grey (right y-axis values). The y-axis values differ between graphs (a-b) and (c).

903

904



906 **Fig. 9** Reliability diagrams (observed frequency for binned forecast probabilities) for September mean
 907 SIC exceeding the 0.15 threshold computed for grid cells of the Beaufort-Chukchi seas region, using
 908 trend-adjusted (a-d) and bias-corrected (e-h) SIC ensemble re-forecasts initialized in May 1993-2014
 909 for the three operational systems and the C3S MME. The size of the dots is proportional to the
 910 population of each bin. Reference data is NSIDC. The Brier Skill Score as well as reliability and
 911 resolution components of the Brier Score are shown in the top left corner of each diagram
 912



914 **Fig. 10** Same as Fig. 9 but for the Laptev-East Siberian Seas region

915